Battery Lifetime Extension Using Super capacitors in Small-Scale Wind-Energy System with fuzzy logic control

K.Harinath Reddy, S.Sarada, J.Venkata Ravi Kumar

***Abstract*— Because of the variable attributes of renewable era, batteries utilized as a part of renewable-force frameworks can experience numerous unpredictable, incomplete charge/release cycles. This study shows a technique for enhancing battery lifetime in a little scale remote-zone wind-power framework by the utilization of a battery/super capacitor half breed vitality stockpiling framework. An agent element model of the general framework, consolidating practical wind-speed and load power varieties has been produced.**

***Index Terms*—Wind energy, Battery lifetime extension.**

I. INTRODUCTION

Optional lead-corrosive batteries may have a run of the mill administration life of under 1000 full-cycles and regularly constitute an expansive extent of the aggregate expense of a renewable vitality venture. The point of this study is to add to a framework to drag out anticipated battery lifetime, along these lines decreasing battery-substitution costs. This can be a huge point of preference, especially in remote ranges, where access can be troublesome and expensive. As opposed to optional batteries, super capacitors additionally known as "electrochemical twofold layer capacitors" (EDLC), or "ultra capacitors," offer higher force thickness and expanded cycle life (of the request of 106 cycles) yet have an extensively lower vitality thickness. Consolidating two or more vitality stockpiling frameworks allows the advantageous credits from every gadget to be used.

II. FRAMEWORK DESCRIPTION

To show the proposed framework, a sample low power (<10 kW) and low battery voltage (<48 Vdc) wind vitality change framework arranged, as appeared in Fig. 1, was considered. In it, the created air conditioning voltage from the wind-turbine is corrected what's more, sustained to the battery and burden by means of a dc/dc converter working under greatest force point following (MPPT) control,

K.Harinath Reddy, Assistant Professor, Department of Electrical & Electronics Engineering, Annamacharya Institute of Technology & Sciences, Rajampet, Andhra Pradesh , India.

S.Sarada, Assistant Professor, Department of Electrical & Electronics Engineering, Annamacharya Institute of Technology & Sciences, Rajampet, Andhra Pradesh , India.

J.Venkata Ravi Kumar, PG Student, Department of Electrical & Electronics Engineering, Annamacharya Institute of Technology & Sciences, Rajampet, Andhra Pradesh , India.

III. CURRENT-CONTROLLED DC/DC CONVERTER

Because of turbulent wind power varieties and short-term load varieties, batteries can be relied upon to experience regular charge/release cycling in remote-range wind-power

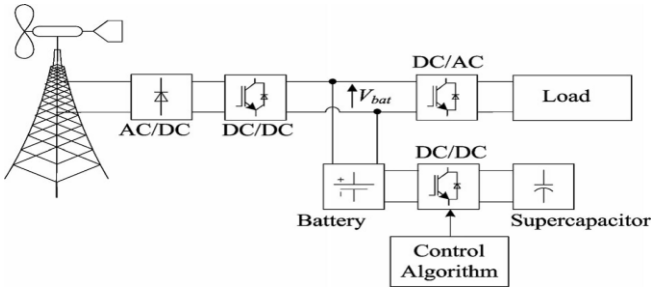

Fig. 1. Remote wind-energy conversion system configuration.

The dc/dc converter under the proposed control system channels transient varieties from the battery charge-profile progressively by occupying them to/from the super capacitor module. Hysteretic current-mode control can be utilized to keep up tight regulation of the inductor current in dc/dc converters and gives powerful execution in spite of variety and instability in working conditions. Furthermore, this control procedure succeeds the sub harmonic swaying unsteadiness that happens at obligation proportions above half with routine PWM current-mode control which requires the included intricacy of incline pay to determine.

A. Current-Controlled DC/DC Converter

Expecting perfect segments, the representing comparison for the inductor current in the converter of Fig. 2 is:

$$L\frac{dI_L}{dt} = V_{sc}.u - V_{bat}. \quad (1)$$

The present's target controller for this situation is to keep up the converter yield current by managing the inductor current to track the order reference current I∗. This is finished by regulating the force electronic switch control signal, u, utilizing the accompanying technique

$$\sigma = I_L - I^* = 0 \quad (2)$$

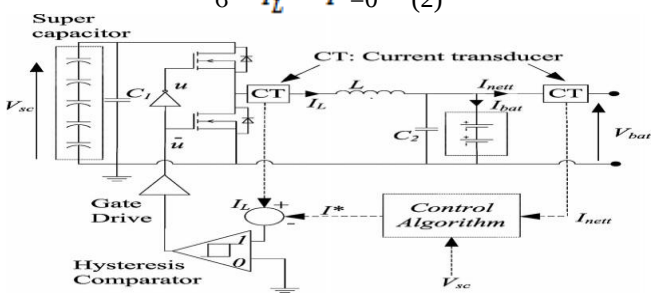

Fig. 2. DC/DC converter and controller.

A switch control system for the sign u (see Fig. 2) can be decided to fulfill (3) such that σ and its time subsidiary have

inverse signs. This guarantees that the framework will join to the state σ = 0 and thusly the normal inductor current joins to the set-point current reference I*

$$\forall \sigma \neq 0 : \sigma . \frac{d\sigma}{dt} < 0. \quad (3)$$

An exchanging control law, which fulfills condition (3), is characterized in (4), where 2h is a little steady hysteresis band (100 mA for this situation),

$$u = \begin{cases} u = 1, if \sigma < -h \\ u = 0, \ if > h \end{cases} \quad (4)$$

For later power conversion efficiency estimation, the approximate switching frequency few can be determined from the inductor rise and fall times (*T*1 and *T*2) in each switch position from (1) as follows.

$$F_{sw} = \frac{1}{T_1 + T_2} = \frac{1}{(2hL/(V_{sc} - V_{bat})) + (-2hL/-V_{bat}}. \quad (5)$$

B. *Control Algorithm*

The control calculation was executed utilizing a dynamic current-sifting way to deal with direct the high-recurrence part of the framework charge/release current Inet to the super capacitor, progressively. The controller constantly screens the episode battery current Inet and sets the converter current reference current I* to scratch off the high-recurrence segment of Inet as appeared in Fig. 3. Self-release causes vitality put away in the super capacitor to rot.

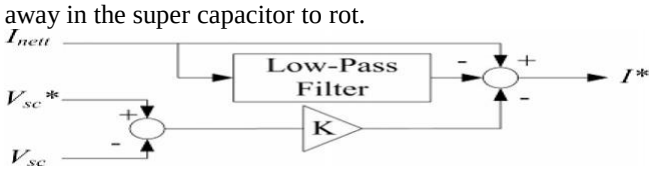

Fig. 3. Control algorithm block diagram.

C. *Test Results*

A model test framework was developed comprising of four 12 Vdc/75 Ah fixed lead-corrosive batteries designed with a 24 Vdc ostensible voltage. The super capacitor module was made up of twenty two 2.7 Vdc, 1800 F Boost cap super capacitor cells (from maker Maxwell Technologies joined in arrangement, giving a 60 Vdc ostensible voltage. It is past the extent of this report to depict the wind turbine furthermore, stack emulator in point of interest; be that as it may, they were executed in equipment utilizing force electronic converters with adequate force control data transfer capacity to speak to the test's way profiles utilized.

IV. FRAMEWORK SIMULATION

To empower battery-life examination over longer periods than would be viable by test, Traditional recreations utilizing mean information for renewable asset designs have been appeared to bring about fleeting changes and related charge/release cycles to be disregarded, bringing about underestimation of battery throughput and related wear

A. *Battery Model*

The dynamic battery model portrayed was utilized to speak to battery voltage and condition of charge (SOC) varieties.

$$C(I, \theta) = \frac{K_c C_0 \left(1 + \frac{\theta}{\theta_f}\right)^{\varepsilon}}{1 + (K_c - 1)(I/I^*_{nom})^K} \quad (6)$$

A nitty gritty portrayal of the demonstrating parameter ID procedure is given. With the end goal of this recreation, the battery parameters accommodated charge and release

$$soc = 1 - \frac{Q_e}{c(0,\theta)} \ Where \ Q_e = \int_0^t -I_m(t)dt \quad (7)$$

$$DOC = 1 - \frac{Q_e}{C(I_{fil},\theta)} \ Where \ I_{fil} = I_m/(1 + T_{bs}) \quad (8)$$

$$E_m(soc) = E_{m0} + K_E(273 + \theta)ln(SOC) \quad (9)$$

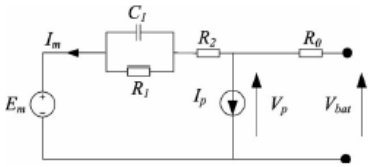

$$R_0(\text{SOC}) = R_{00}[1 + A_0(1 - SOC)] \quad (10)$$

$$R_1 = -R_{10}\ln(DOC) \quad (11)$$

$$R_2 = R_{20}\frac{\exp[A_{21}(1 - SOC)]}{1 + \exp(A_{22}I_{m/I^*})} \quad (12)$$

$$I_p = V_{pn}G_{p0}\exp\left[\frac{V_{pn}}{V_{p0}} + A_p\left(1 - \frac{\theta}{\theta_f}\right)\right] \quad (13)$$

B. *Super capacitor Model*

Super capacitor powerful capacitance can be portrayed by a nonlinear capacity of terminal voltage. On the other hand, in this study; the improved model of Fig. 6 was utilized. The powerful capacitance C*, the spillage resistance Rleak, and the arrangement resistance Rest terms can be dictated by estimation alternately got from producer's information.

$$V_{sc} = \frac{1}{C^*}\int\left(I_{sc} - \frac{V_{sc}}{R_{leak}}\right)dt + I_{sc}R_{esr}. \quad (14)$$

The required super capacitor vitality stockpiling limit was resolved observationally by reenactment. The super capacitor module was then designed utilizing a blend of standard industrially accessible super capacitor cells with parameters given in the Appendix; see Table AII. The powerful aggregate capacitance C∗ and arrangement and spillage resistances (Rleak and Resr) were ascertained in view of the quantity of arrangement/parallel super capacitor cells.

C. *Converter Model*

Because of the recreation's length interim of one week, an arrived at the midpoint of converter model was created.

It was important to evaluate the converter changing recurrence from (5) for exchanging misfortune estimation. The effectiveness model depended on that created in and can be outlined as takes after.

$$P_{conduction} = I_{out}^2 + R_{ds(on)} + I_{out}^2 R_L \quad (15)$$

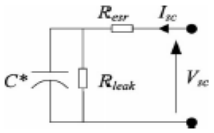

$$P_{switching} = 0.5V_{sc}I_{out}(t_r + t_f)f_{sw} + 0.5C_{OSS}V_{sc}^2 f_{sw} + Q_{rr}V_{sc}f_{sw} \quad (16)$$

The primary term speaks to power lost because of voltage/current cover amid the rising and falling exchanging interim (tr also, tf). The second term speaks to the force misfortune related with charging the MOSFET yield capacitance Coss. The third term speaks to the misfortune connected with the MOSFET bodydiode reverse recuperation charge Qrr . The suspicion has been made in (16) that

exchanging misfortunes in the influence MOSFET with the dynamic characteristic diode forward one-sided are unimportant, since exchanging happens with a diode volt drop connected over the switch. A significant number of the past misfortune parameters are temperature dependent what's more, an exact reproduction would demonstrate these conditions. Rather, to give an estimation of the converter misfortunes, assuming the worst possible scenario, and (most extreme) datasheet values for T_r, T_f, C_{oss}, also, Q_{rr} were utilized. The inductor current positive and negative slew-rate limits can be resolved from (2) as takes after:

$$\left(\frac{di}{dt}\right)_{rise} = \frac{V_{sc}-V_{bat}}{L}\left(\frac{di}{dt}\right)_{fall} = \frac{-V_{bat}}{L}. \quad (17)$$

D. Wind Profile Model

A cross breed methodology was utilized to portray element wind-speed varieties with the low-recurrence segment of the wind speed described utilizing promptly accessible genuine meteorological wind-speed information taken at 1800s examining interims at a neighborhood climate station. To depict the way of transient wind-speed varieties, a reenacted high-recurrence or turbulent wind-speed segment was superimposed onto the half hourly wind-speed information in view of the system portrayed. For this situation, the ghostly properties of the von Karman turbulence model were depicted in the recurrence area utilizing an exchange capacity Ht (s) of the accompanying structure:

$$H_t(s) = K_f \frac{m_1 T_{fs}+1}{(T_{fs}+1)(m_2 T_{fs}+1)} \quad (18)$$

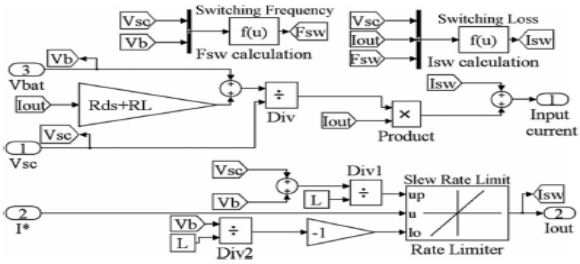

Fig. 7. Averaged Simulink model of a hysteretic current-controlled dc/dc Converter.

where m_1 = 0.4 and m_2 = 0.25.For each measured value of the quasi-steady half-hourly "mean" wind speed, V_{mean}, the time parameter T_f and gain K_f were computed as follows:

$$T_f(t) = {}^{L_t}/_{v_{mean}(t)} \quad (19)$$

$$K_f = \sqrt{\frac{2\pi.T_f}{\beta\left(\frac{1}{2},\frac{1}{3}\right).T_s}} \quad (20)$$

Where Ts is the example time (for this situation 1 s) and β means the beta capacity.

A background noise was utilized as the info to the "molding channel" given by (18) and the signal's change at the yield of the forming channel was balanced by the variable It mean. It is the turbulence force variable at the site being referred to what's more, has been accepted to have an estimation of 0.1 in the accompanying reproduction. The turbulent wind-speed part model can be executed in MATLAB/Simulink as appeared in Fig. 8. The general wind-pace is the whole of the semi unfaltering half hourly "signify" and the turbulent part. The suspicion has been made that this speaks to the whole wind field acting on the rotor cleared zone, since this study considers a class of wind turbines with generally little cutting edge distance across (<10 m). This is upheld in pertinent writing E. Wind-Turbine Model the wind-turbine model was proposed to catch the predominant motion of the wind-turbine force yield with exchanging and electromagnetic homeless people dismissed. The force created by the wind-turbine rotor can be composed as

$$P_{wind} = 0.5C_p(\lambda)\rho A v_{wind}^3 \quad (21)$$

where ρ is the air thickness in (kg/m^3), An is the rotor cleared range (m2), λ is the proportion of cutting edge tip pace to center point rotational speed, furthermore, vwind is the episode wind speed (m/s).

$$C_p = C_1(C_2 - C_3\theta - C_4\theta^x - C_5)e^{-C_6} \quad (22)$$

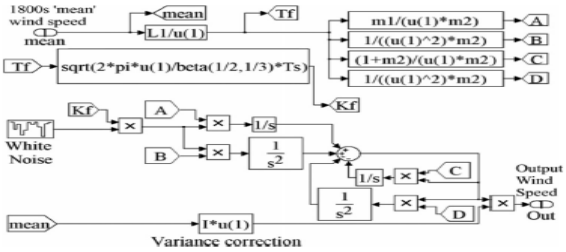

Fig. 8. Simulink implementation of the von Karman turbulence model (*Ts* =1 s, turbulence simulation sample time).

Where *C*1 = 5176, *C*2 = 116/ *λi, C*3 = 0.4, *C*4 = 0, *C*5 = 5, and *C*6 = 21/*λi. λi* is a function of the tip speed ratio and the pitch angle:

$$\frac{1}{\lambda_i} = \frac{1}{\lambda + 0.089} - \frac{0.035}{\theta^3 + 1}. \quad (23)$$

The torque developed by the wind turbine can then be expressed as:

$$T_{wind} = \frac{P_{wind}}{\omega} \quad (24)$$

where ω is the pole rotational speed (rad/s).A MPPT calculation as depicted in directs the force conveyed by the wind-turbine generator and force electronic converter.

$$\lambda_{opt} = \frac{R\omega}{v_{wind}} \quad or \; v_{wind} = \frac{R\omega}{\lambda_{opt}} \quad (25)$$

where *R* = blade radius (m) and *v*wind = incident wind speed (m/s).Substituting (25) into (21) and using relation (24) yields the optimal power reference *P*opt and resulting electromagnetic torque *T*em as a function of *ω*:

$$T_{em} = \frac{P_{opt}}{\omega} = \frac{0.5C_p(\lambda_{opt})\rho\pi R^5}{\lambda_{opt}^3}\omega^2 \quad (26)$$

The aggregate idleness and damping of the wind turbine and generator mechanical subsystem are depicted by the idleness Jwhat's more, damping D coefficients.

The MPPT calculation depicted sets the force yield of the electrical subsystem based on the pole speed, to the ideal worth Popt.

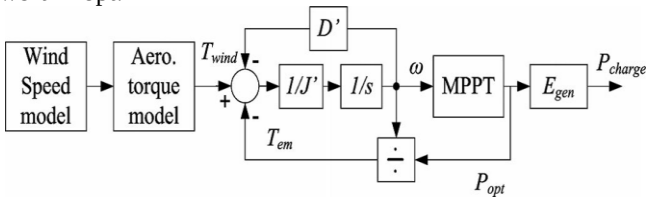

Fig. 9. Wind-turbine model top-level block diagram.

Parameters). The general wind-turbine demonstrating methodology is outlined by the top-level graph in Fig. 9. F. Burden Model The heap profile of a low-use local home was logged through the span of a day.

V. BATTERY LIFETIME MODELING

To survey the execution of the proposed framework, a battery life cycle estimation system in light of the strategies portrayed was created.

$$C_d = a_1 d^{-4} + a_2 d^{-3} + a_3 d^{-2} + a_4 d^{-1} + a_5$$
$$a_1 = -1.345 \times 10^{-12} \quad a_2 = 1.495 \times 10^{-7}$$
$$a_3 = -0.001507 \quad a_4 = 601.5 \quad a_5 = -122.5 \quad (27)$$

Where d=depth of release and Cd =cycles to disappointment at profundity of released.

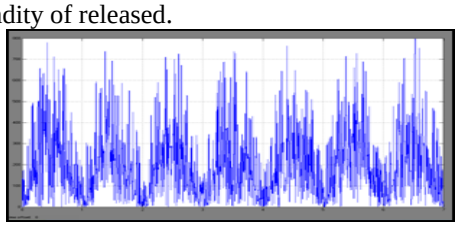

Battery only system results: battery current

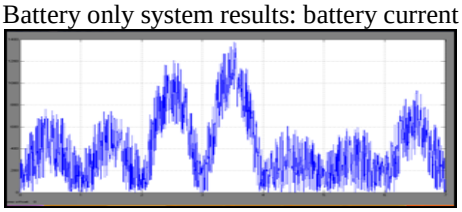

Battery state of charge,

The system known as "downpour flow counting," likewise utilized as a part of metal exhaustion estimation and depicted was connected to number the number of sporadic, covering cycles, and half-cycles for each "profundity" range.

$$w = \sum_{i=i_{min}}^{i=i_{max}} \frac{N_i}{C_{di}} \quad (28)$$

$$Life(days) = \frac{N_{days}}{W}. \quad (29)$$

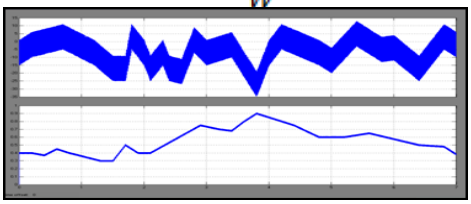

Battery only system results: battery current, battery state of charge.

VI. RESULTS AND DISCUSSION

The SOC of the battery in the crossover framework experiences less charge/release cycles. The consequences of downpour stream numbering of the battery SOC profile measures the quantity of charge/release cycles experienced by the battery in every framework. that the battery SOC in the cross breeds framework experiences widely less short-range cycles.

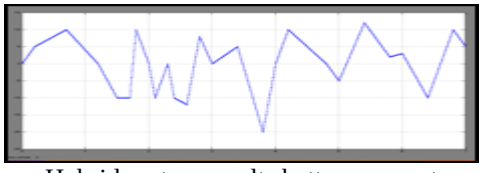

Hybrid system results battery current

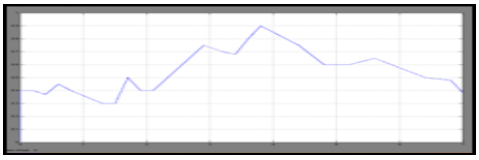

Hybrid system battery state of charge.

Extension results:

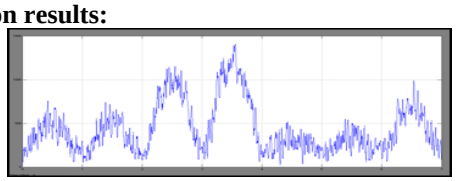

Battery only system results battery current

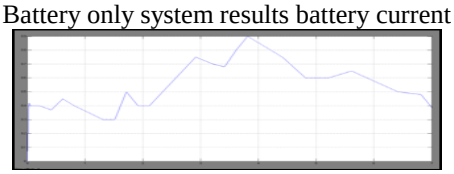

Battery state of charge,

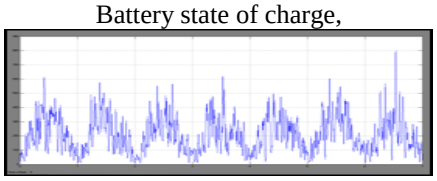

Battery state of charge,

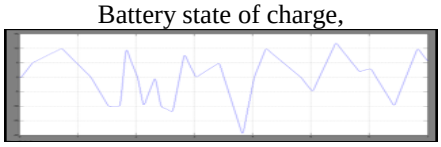

Battery state of charge

VII. CONCLUSION

This study has explored the utilization of super capacitors to move forward expected battery life cycle over an agent weeklong force profile run of the mill of a little, remote-zone wind-vitality change framework. The outcomes demonstrate that by redirecting transient power varieties because of turbulence and fleeting burden varieties to a super capacitor module, battery life cycle can be quantifiably expanded. It has additionally been demonstrated that the battery current maxima can be essentially decreased utilizing the proposed framework. This has an unmodeled advantage regarding possibly facilitate expanding battery life as high-current cycling has been appeared to build battery disappointment rates.

REFERENCES

[1] N. Kularatna,"Rechargeable batteries and their management,"IEEE Instrum.Meas. Mag., vol. 14, no. 2, pp. 20–33, Apr. 2011.

[2] S. Vazquez, S. M. Lukic, E. Galvan, L. G. Franquelo, and J. M. Carrasco,"Energy storage systems for transport and grid applications," IEEE Trans.Ind. Electron. vol. 57, no. 12, pp. 3881–3895, Dec. 2010.

[3] L. Peiwen, "Energy storage is the core of renewable technologies, Nanotechnol.Mag" vol. 2, no. 4, pp. 13–18, Dec. 2008.

[4] Q. Liyan and Q. Wei, "Constant power control of DFIG wind turbines with super capacitor energy storage," IEEE Trans. Ind. Appl., vol. 47,no. 1, pp. 359–367, Jan. 2011.

[5] M. Uzunoglu and M. S. Alam, "Dynamic modeling, design, and simulation of a combined PEM fuel cell and ultra capacitor system for stand-alone residential applications," IEEE Trans.